

Realistic Kidney Simulation for the Development of Renal Function Diagnostics by Dynamic SPECT Imaging

Ákos Szlávecz * Bálint Szabó * Balázs Benyó *

* *Department of Control Engineering and Information Technology, Budapest University of Technology and Economics, Budapest, Hungary*

Abstract: Dynamic SPECT imaging captures the dynamic process of the radioisotope washed in and out, to and from tissues and exchanged between biological compartments. One of the most common application field for dynamic SPECT imaging is investigating renal functions. The main goal of this study was to create realistic simulations of the kidney in order to support the development of dynamic SPECT reconstruction algorithms. We created and parametrized a compartment model of the kidney for simulating the dynamic behavior of the MAG3 radiopharmakon. Solving the model with a parameter set corresponding to the normal and to the pathological cases the SPECT data acquisition was simulated using the GATE Monte Carlo simulation toolkit.

Keywords: SPECT, Dynamic SPECT, MAG3, Compartment model, Simulation, GATE

1. INTRODUCTION

2. METHODS

Single Photon Emission Computed Tomography (SPECT) is a widely used nuclear imaging technique for functional imaging (Wernick and Aarsvold (2004)). In conventional SPECT imaging, the administered radiotracer distributes in the body and remains stationer during the examination. The dynamic SPECT imaging captures the dynamic process of the radiotracer washed in and out, to and from tissues and exchanged between biological compartments. Determining kinetic parameters of the dynamic process could improve diagnosis in different application fields such as myocardial, renal, and brain studies (Iskandrian, Abdulmassih S. and Van Der Wall, Ernst E. (1994); Miyazaki et al. (2010); Sitek et al. (2001); Hsu et al. (2014)). One of the most common application field of dynamic SPECT imaging is investigating renal functions.

The main scope of this study is to create a reference dataset that can be used for the development of dynamic SPECT reconstruction algorithms. This reference dataset will be the input of the GATE Monte Carlo simulation toolkit (Jan et al. (2004)) for simulating realistic SPECT renal study. The simulated SPECT study can then be used for testing our dynamic SPECT reconstruction algorithm (Barna et al. (2017, 2018)).

The paper introduces the applied compartment model and the related differential equations, the parameter set for normal and pathological cases, and the SPECT simulation of a dynamic data acquisition.

2.1 Modeled Physiological Phenomenon

The kidneys are two bean-shaped organs located on the left and right in the retroperitoneal space. They receive blood from the paired renal arteries. The kidney is divided in two major parts: cortex and medulla. It receives blood from the paired renal arteries. Each renal artery branches into segmental arteries, dividing further into interlobar arteries, which penetrate the renal capsule and extend through the renal columns between the renal pyramids. The interlobar arteries then supply blood to the arcuate arteries that run through the boundary of the cortex and the medulla. Each arcuate artery supplies several interlobular arteries that feed into the afferent arterioles that supply the glomeruli.

After filtration occurs, the blood moves through a small network of venules that converge into interlobular veins. As with the arteriole distribution, the veins follow the same pattern: the interlobular provide blood to the arcuate veins then back to the interlobar veins, which come to form the renal vein exiting the kidney for transfusion for blood.

Each kidney is attached to a ureter, a tube that carries excreted urine to the bladder. The kidney is responsible to filter substances from the blood which takes place at the renal corpuscle. By this process cells and large proteins are retained in the blood flow while materials of smaller molecular weights are filtered from the blood to make an ultrafiltrate that becomes urine.

Tc99m-MAG3 radioisotope is commonly used for investigating renal function. The MAG3 clearance is highly correlated with the effective renal plasma flow (ERPF),

* The research was supported by the Hungarian National Scientific Research Foundation, Grant No. K116574, by the NRDI Fund (TKP2020 IES, Grant No. BME-IE-BIO) and by H2020 MSCA-RISE DCPM (#872488) grant.

and the MAG3 clearance can be used as an independent measure of renal function.

In clinical examinations the renal function is generally visualized in a renogram. A renogram is simply a time-activity curve that provides a graphic representation of the uptake and excretion of a radiopharmaceutical by the kidneys. A typical renogram curve of a normal kidney function is shown in Figure 1. The renogram shows symmetric activity between the right and left kidney, rapid drop-off after the peak, and a long tail extending to the right. There is an increasing activity within the bladder after about 4 minutes.

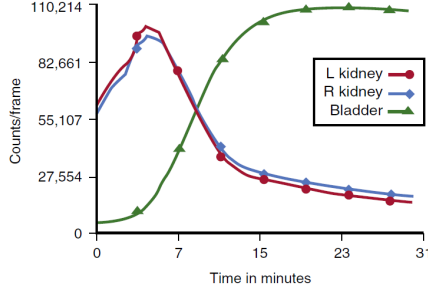


Fig. 1. Renogram: normal kidney. (Mettler and Guiberteau (2012))

The MAG3 radioisotope is usually used for diagnosing the following pathological renal cases (Bennett (2016) Mettler and Guiberteau (2012)).

- Vesicoureteral reflux (Bennett (2016); Mettler and Guiberteau (2012))

In normal patients, no radiopharmaceutical reflux from the bladder into the ureters or the kidneys is seen. In case of vesicoureteral reflux, due to malfunction, there is a flow of urine from bladder into ureter and/or renal pelvis (Figure 2).

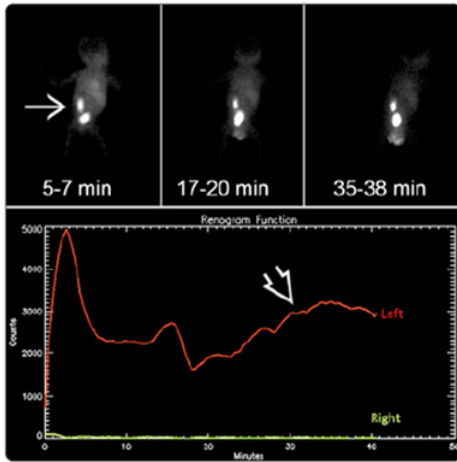


Fig. 2. Renogram: vesicoureteral reflux. (Bennett (2016)) Radiotracer in the left renal collecting system increases over time due to vesicoureteric reflux.

- Functional obstruction (Mettler and Guiberteau (2012))

In case of functional obstruction the urine flow into the bladder is blocked. As a consequence of this, the urine production and the radiopharmakon cannot

be excreted through the bladder. In the renogram a delayed excretion can be observed (Figure 3).

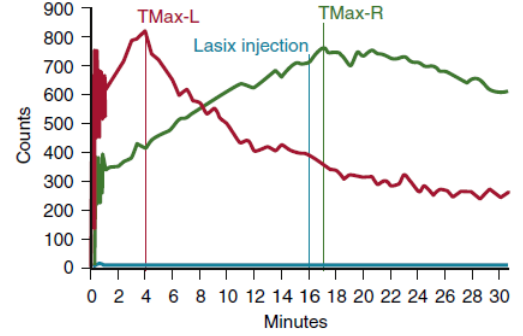


Fig. 3. Renogram: functional obstruction. (Mettler and Guiberteau (2012)) Time-activity curves show the normal excretion on the left (red curve) and delayed excretion on the right (green curve).

2.2 The compartment model of the kidney for MAG3

Brolin et al created a compartmental model for modeling the dynamic behavior of the MAG3 isotope for simulating MAG3 pharmacokinetics (Brolin et al. (2013)).

The model is composed of single compartments (open boxes) and delay functions (shadowed boxes), where the latter consist of a number of internal compartments linked in series (Figure 4). The left and right kidneys are structurally composed of the renal cortex, medulla, and pelvis. The cortex and medulla are modeled by delay functions to allow for realistic renal transit time distributions.

The compartment model shown in Figure 4 is described by a system of first-order linear differential equations, as follows:

$$\frac{dC_i(t)}{dt} = \frac{1}{V_i} \sum_{j=1}^N (r_{j \rightarrow i} C_j(t) - r_{i \rightarrow j} C_i(t)) \quad (1)$$

where $C_i(t)$ is the tracer concentration in compartment i at time t , V_i is the volume of the i th compartment, $r_{j \rightarrow i}$ is the transfer rate constant from compartment j to i in unit volume per unit time, and N is the number of compartments in the model.

Equation (1) can also be written as:

$$\frac{dA_i(t)}{dt} = \sum_{j=1}^N (k_{j \rightarrow i} A_j(t) - k_{i \rightarrow j} A_i(t)) \quad (2)$$

where $A_i(t) = C_i(t) \cdot V_i$ is the total tracer amount in compartment i , and the transfer rate constants $k_{j \rightarrow i} = V_{j \rightarrow i}$ are given in units of reciprocal time.

The model of the tracer transport through the renal cortex and medulla is shown in Figure 4(b). To allow manipulation of the transit time distribution through the kidneys, delay functions are used. These are characterized by a mean transit time τ and a shape parameter m , and are constructed by linking m internal compartments in series with internal transfer rate constants r_{int} , given by

$$r_{int} = \frac{m}{\tau} \cdot V_{int} \quad (3)$$

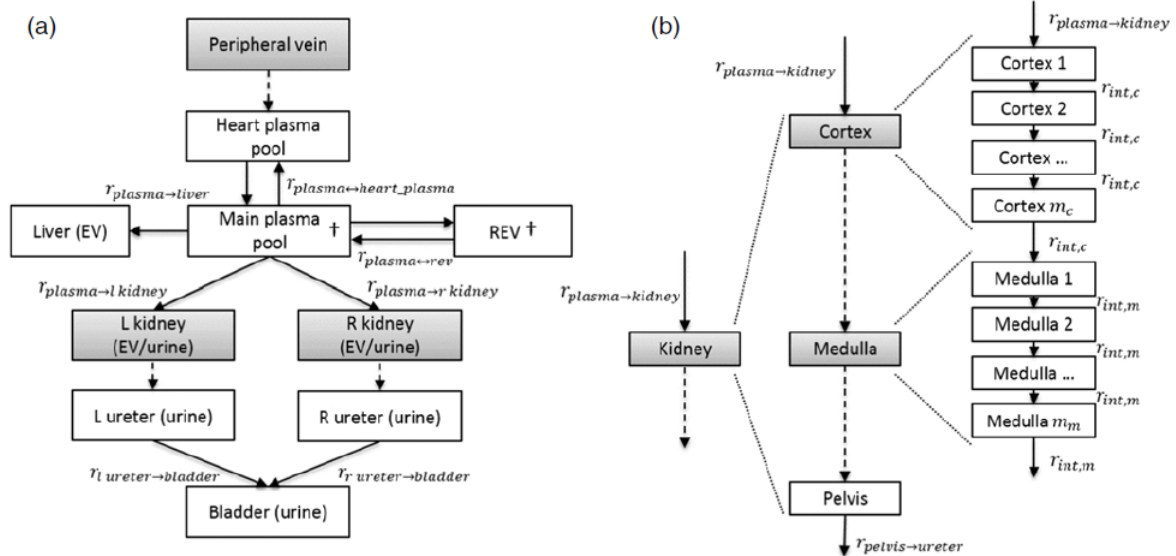


Fig. 4. (a) The MAG3 compartment model (Brolin et al. (2013)). Solid arrows represent first-order transfer rate constants ($r_{i \rightarrow j}$) and dashed arrows indicate the direction of transfer from one (or several) delays. Compartments without structural counterparts in the phantom are the plasma pool and the rest-of-body extravascular (REV) space, as marked with (\dagger). (b) The left and right kidneys are structurally composed of the renal cortex, medulla, and pelvis. The cortex and medulla are modeled by delay functions to allow for realistic renal transit time distributions.

where V_{int} is the volume of the internal compartments.

The applied compartment volumes and the baseline parameter values used for simulating a normal subject are summarized in Table 1 and Table 2 correspondingly.

Compartment	Volume (ml)
Heart plasma	170
Main plasma	2495
Extravascular space	2664
Liver	874
Left renal pelvis	6
Right renal pelvis	5
Left ureter	4
Right ureter	4
Bladder	46

Table 1. Compartment volumes.

Parameter	Value
$r_{plasma \leftrightarrow heartplasma}$	$3200 \frac{ml}{min}$
$r_{plasma \rightarrow liver}$	$14 \frac{ml}{min}$
$r_{plasma \leftrightarrow REV}$	$250 \frac{ml}{min}$
$r_{plasma \rightarrow kidneys}$	$130 \frac{ml}{min}$
τ_{cortex}	$1.25min$
m_{cortex}	20
$\tau_{medulla}$	$1.25min$
$m_{medulla}$	20
$r_{pelvis \rightarrow ureter}$	$4 \frac{ml}{min}$
$r_{ureter \rightarrow bladder}$	$15 \frac{ml}{min}$

Table 2. Baseline MAG3 kinetic parameter values.

3. RESULTS

3.1 Compartment model parameters for normal and pathological cases

The compartment model shown in Figure 4, described by the Equations (1)-(3) has been implemented. The kinetic

parameter values in Table 2 were modified in order to simulate a kidney for normal and different pathological cases. For normal kidney the original flow rates have been used shown in Table 2. The compartment model has been solved using the 4th order Runge-Kutta method. The simulated renogram curves are displayed in Figure 5.

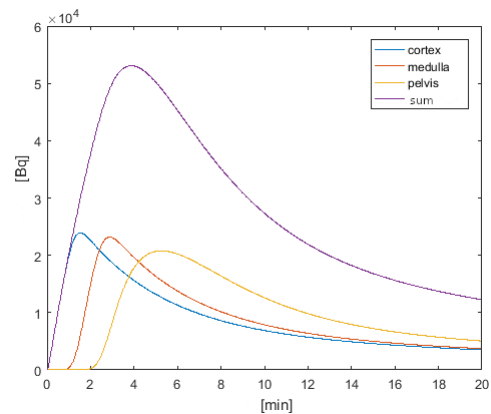


Fig. 5. Simulated renogram based on the compartment model: normal kidney.

Simulation of vesicoureteral reflux In case of vesicoureteral reflux there is flow from the ureter to pelvis. In order to simulate this kind of pathological behavior we had to modify the compartment model. A new flow rate was introduced in the compartment model in direction from the bladder to the ureter ($r_{bladder \rightarrow ureter}$) and from the ureter to the pelvis ($r_{ureter \rightarrow pelvis}$). The reflux happens if the pressure is enough high to initiate the flow of urine back to the pelvis. This develops usually after 10 minutes of the beginning of the study, thus, in the simulation a timing was implemented that starts the activates the backward flow rates. The compartment model has been

solved using the 4th order Runge-Kutta method using the parameters in Table 3. The simulated renogram curves are displayed in Figure 6.

Parameter	Original value	Modified value
$r_{plasma \leftrightarrow heartplasma}$	$3200 \frac{ml}{min}$	-
$r_{plasma \rightarrow liver}$	$14 \frac{ml}{min}$	-
$r_{plasma \leftrightarrow REV}$	$250 \frac{ml}{min}$	-
$r_{plasma \rightarrow kidneys}$	$130 \frac{ml}{min}$	-
τ_{cortex}	$1.25min$	-
m_{cortex}	20	-
$\tau_{medulla}$	$1.25min$	-
$m_{medulla}$	20	-
$r_{pelvis \rightarrow ureter}$	$4 \frac{ml}{min}$	-
$r_{ureter \rightarrow bladder}$	$15 \frac{ml}{min}$	-
$r_{ureter \rightarrow pelvis}$	-	$14 \frac{ml}{min}$
$r_{bladder \rightarrow ureter}$	-	$5 \frac{ml}{min}$

Table 3. MAG3 kinetic parameter values used for simulating vesicoureteral reflux.

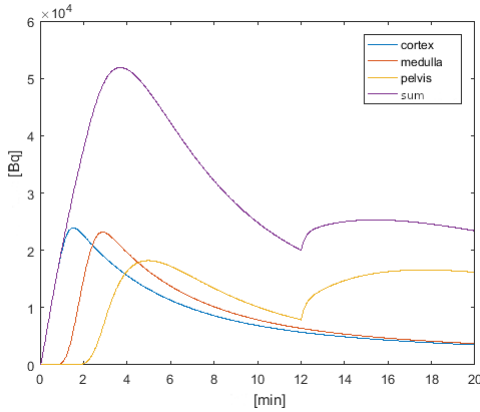


Fig. 6. Simulated renogram based on the compartment model: vesicoureteral reflux.

Simulation of functional obstruction In case of functional obstruction the way to the ureter and the bladder is blocked, the filtrated substance can not be extracted with the proper flow rate resulting in a delayed activity curve. We can simulate this behavior by changing the delay rates of the cortex and medulla and the flow rates from the pelvis to the ureter and from the ureter to the bladder. The new flow rates can be found in Table 4. The compartment model has been solved using the 4th order Runge-Kutta method using the parameters in Table 4. The simulated renogram curves are displayed in Figure 7.

Parameter	Original value	Modified value
$r_{plasma \leftrightarrow heartplasma}$	$3200 \frac{ml}{min}$	-
$r_{plasma \rightarrow liver}$	$14 \frac{ml}{min}$	-
$r_{plasma \leftrightarrow REV}$	$250 \frac{ml}{min}$	-
$r_{plasma \rightarrow kidneys}$	$130 \frac{ml}{min}$	-
τ_{cortex}	$1.25min$	1.75 min
m_{cortex}	20	-
$\tau_{medulla}$	$1.25min$	1.75 min
$m_{medulla}$	20	-
$r_{pelvis \rightarrow ureter}$	$4 \frac{ml}{min}$	$0.5 \frac{ml}{min}$
$r_{ureter \rightarrow bladder}$	$15 \frac{ml}{min}$	$4 \frac{ml}{min}$

Table 4. MAG3 kinetic parameter values used for simulating functional obstruction.

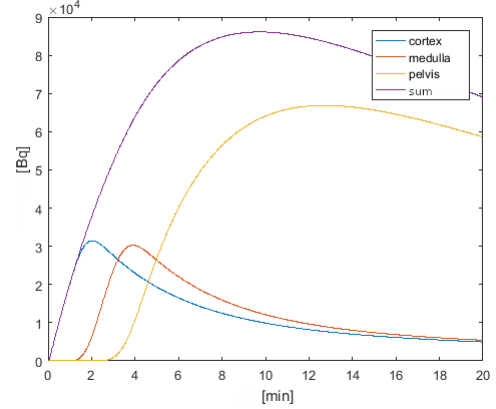


Fig. 7. Simulated renogram based on the compartment model: functional obstruction.

3.2 SPECT simulation using the GATE Monte Carlo simulation toolkit

We have created a voxelized mathematical kidney phantom derived from CT scan that contains the details: aorta, left cortex, left medulla, left pelvis, left ureter, right cortex, right medulla, right pelvis, right ureter, and the bladder. Time activity curves has been created for a normal kidney and for obstruction based on the compartmental model described above. The time activity curves and the voxelized mathematical phantom were used for input to the GATE simulation toolkit. In the simulation we used a small animal SPECT system with 4 heads equipped with multi pinhole collimators and list mode data were collected.

GATE simulation of normal kidney Figure 8 displays the result of the GATE simulation. Decay positions of the gamma photons were binned in a voxelized space according to the mathematical phantom. Every image on the left shows a summed time interval of decay positions. The right curve displays the simulated time activity curve marked with the corresponding time interval.

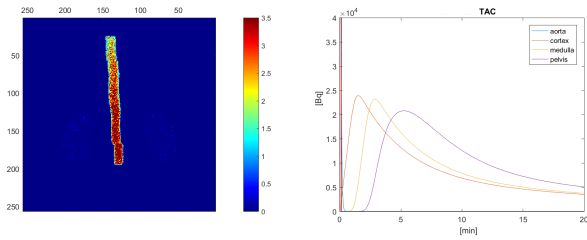
GATE simulation of functional obstruction Figure 9 displays the result of the GATE simulation. Decay positions of the gamma photons were binned in a voxelized space according to the mathematical phantom. Every image on the left shows a summed time interval of decay positions. The right curve displays the simulated time activity curve marked with the corresponding time interval.

4. DISCUSSION

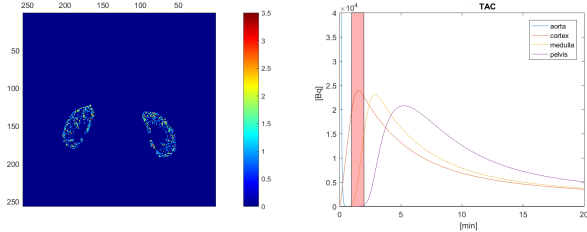
Using the compartment model created for the MAG3 radioisotope we have created time activity curves that corresponds with renograms in clinical studies for both normal and pathological cases.

The compartment model provided realistic renograms as it can be seen in the normal case. The simulated time activity curves in Figure 5 look very similar to the clinical case shown in Figure 1.

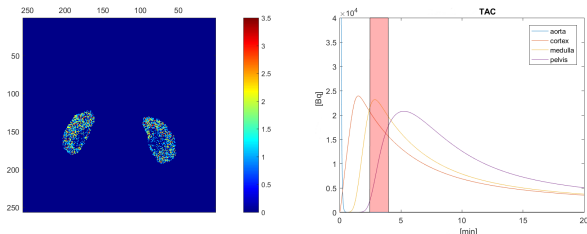
In case of vesicoureteral reflux the compartment model had to be modified, additional flow rates were introduced between pelvis, ureter, and bladder in order to simulate



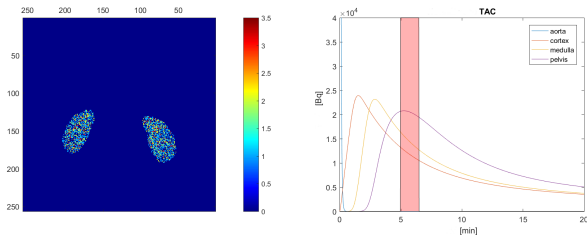
(a) First 15 seconds



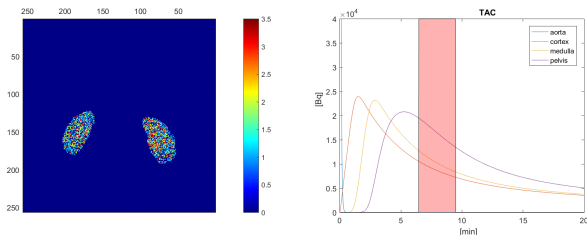
(b) 1.5-2.5 minutes



(c) 3-4.5 minutes



(d) 5.5-7 minutes

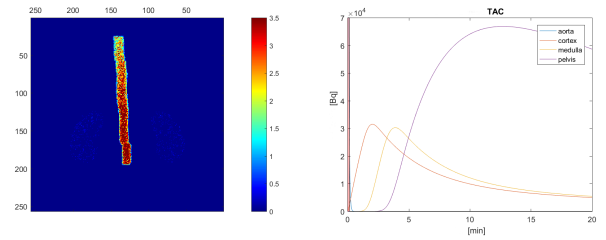


(e) 7-10 minutes

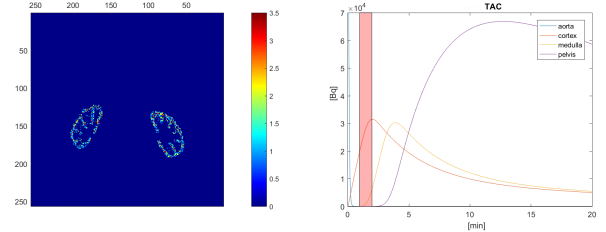
Fig. 8. GATE simulation of the normal kidney.

flow of urine back to the kidney. In this case the simulated renogram shows increased activity in the pelvis when reflux effect starts (Figure 6). This increased activity in the pelvis results in an increased activity in the kidney. In the simulation the start of increasing looks a bit sudden but the renogram is very similar to the clinical case (Figure 2), the difference can be caused by the noise of the real data acquisition in the human examination.

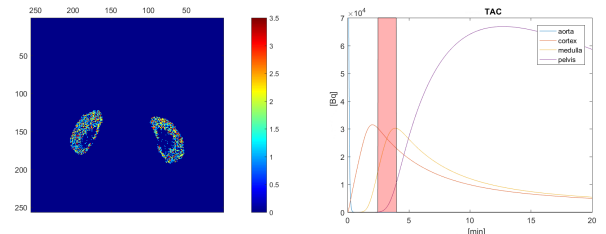
In case of obstruction the outflow of urine is blocked functionally, resulting in a delayed extraction. The activity in the pelvis and consequently in the kidney remains high



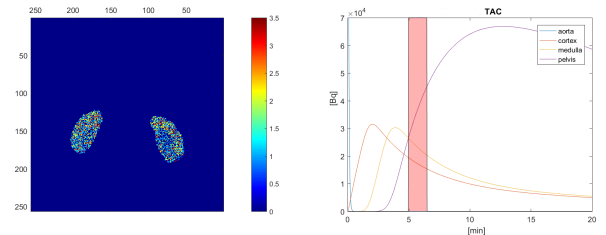
(a) First 15 seconds



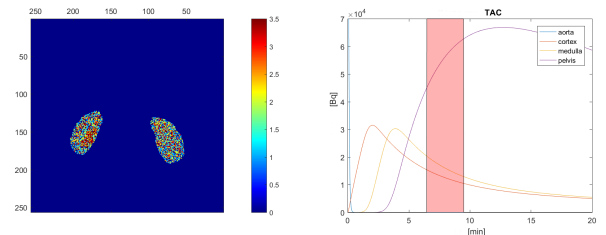
(b) 1.5-2.5 minutes



(c) 3-4.5 minutes



(d) 5.5-7 minutes



(e) 7-10 minutes

Fig. 9. GATE simulation of the kidney with functional obstruction.

as it can be observed in the clinical study in Figure 3 and correspondingly also in the simulated compartment model in Figure 7.

GATE simulation was executed for normal kidney and for kidney with functional obstruction. Due to small time intervals quite low event counts were recorded in the Figures the incremental sum of the interval is displayed (Figure 8 and 9). In the first 15 seconds (first pass) the activity appears in the aorta. In this phase we have to detect events started in the aorta during simulation. This can be observed in Figure 8(a) and in Figure 9(a). Activity

can be found only in the aorta. In the second phase the radioisotope flow reaches the cortex. Both in Figure 8(b) and in Figure 9(b) this can be observed. Activity can be seen in the cortex (in left images) and some in the medulla but the pelvis remains still empty in this phase. In the third phase the pelvis reaches the highest activity in normal case, in the different anatomical parts there is not a big difference in activity. While in case of functional obstruction activity in the pelvis is higher. In the latest phase the activity is decreasing in the kidney. In normal case this phase is similar to the previous that is also suggested by the renogram. However, in case of functional obstruction the activity in pelvis remains high that can be observed in the image in Figure 9(e).

5. CONCLUSIONS

Using the compartment model developed for the MAG3 radioisotope we have created time activity curves that corresponds with renograms in clinical studies. Compartment model was solved for these studies and two of them (normal case and functional obstruction) were simulated using the GATE Monte Carlo simulation toolkit in order to create realistic dynamic SPECT measurements. These simulation results are essential tools in the development of dynamic SPECT reconstruction algorithms that is our subsequent research goal.

REFERENCES

- Barna, Z., Ákos Szlávecz, Hesz, G., and Benyó, B. (2017). A direct method for reconstructing dynamic spect images. *IFAC-PapersOnLine*, 50(1), 15139–15144. 20th IFAC World Congress.
- Barna, Z., Ákos Szlávecz, Hesz, G., Somogyi, P., Kovács, K., and Benyó, B. (2018). Initial value selection of the model parameters in the curve fitting phase of the dynamic spect imaging. *IFAC-PapersOnLine*, 51(27), 241–246. 10th IFAC Symposium on Biological and Medical Systems BMS 2018.
- Bennett, P. (2016). *Diagnostic Imaging: Nuclear Medicine E-Book*. Diagnostic Imaging. Elsevier Health Sciences.
- Brolin, G., Gleisner, K.S., and Ljungberg, M. (2013). Dynamic99mTc-MAG3 renography: images for quality control obtained by combining pharmacokinetic modelling, an anthropomorphic computer phantom and monte carlo simulated scintillation camera imaging. *Physics in Medicine and Biology*, 58(10), 3145–3161.
- Hsu, B., Chen, F.C., Wu, T.C., Huang, W.S., Hou, P.N., Chen, C.C., and Hung, G.U. (2014). Quantitation of myocardial blood flow and myocardial flow reserve with 99mTc-sestamibi dynamic spect/ct to enhance detection of coronary artery disease. *European Journal of Nuclear Medicine and Molecular Imaging*, 41(12), 2294–2306.
- Iskandrian, Abdulmassih S. and Van Der Wall, Ernst E. (1994). *When is myocardial viability a clinically relevant issue?*, 179–192. Springer Netherlands, Dordrecht.
- Jan, S., Santin, G., Strul, D., Staelens, S., Assié, K., Autret, D., Avner, S., Barbier, R., Bardiès, M., Bloomfield, P.M., Brasse, D., Breton, V., Bruyndonckx, P., Buvat, I., Chatzioannou, A.F., Choi, Y., Chung, Y.H., Comtat, C., Donnarieix, D., Ferrer, L., Glick, S.J., Groiselle, C.J., Guez, D., Honore, P.F., Kerhoas-Cavata, S., Kirov, A.S., Kohli, V., Koole, M., Krieguer, M., van der Laan, D.J., Lamare, F., Largeron, G., Lartzien, C., Lazaro, D., Maas, M.C., Maigne, L., Mayet, F., Melot, F., Merheb, C., Pennacchio, E., Perez, J., Pietrzyk, U., Rannou, F.R., Rey, M., Schaart, D.R., Schmidlein, C.R., Simon, L., Song, T.Y., Vieira, J.M., Visvikis, D., de Walle, R.V., Wieërs, E., and Morel, C. (2004). GATE: a simulation toolkit for PET and SPECT. *Physics in Medicine and Biology*, 49(19), 4543–4561.
- Mettler, F. and Guiberteau, M. (2012). *Essentials of Nuclear Medicine Imaging*. Elsevier Inc.
- Miyazaki, C., Harada, H., Shuke, N., Okizaki, A., Miura, M., and Hirano, T. (2010). 99mTc-DTPA dynamic spect and ct volumetry for measuring split renal function in live kidney donors. *Annals of Nuclear Medicine*, 24(3), 189–195.
- Sitek, A., Gullberg, G.T., Di Bella, E.V., and Celler, A. (2001). Reconstruction of dynamic renal tomographic data acquired by slow rotation. 42(11), 1704–1712.
- Wernick, M. and Aarsvold, J. (2004). *Emission Tomography: The Fundamentals of PET and SPECT*. Elsevier Science.